Evidence for Viscoelastic Effects in Surface Capillary Waves of Molten Polymer Films

Zhang Jiang,[1] Hyunjung Kim,[2] X. Jiao,[3] H. Lee,[2] Y.-J. Lee,[2] Y. Byun,[2] S. Song,[2] D. Eom,[2] C. Li,[4] M. H. Rafailovich,[4] L. B. Lurio,[3] and S. K. Sinha[1,5]

[1]*Department of Physics, University of California at San Diego, La Jolla, California 92093, USA*
[2]*Department of Physics and Interdisciplinary Program of Integrated Biotechnology, Sogang University, Seoul 121-742, Korea*
[3]*Department of Physics, Northern Illinois University, DeKalb, Illinois 60115, USA*
[4]*Department of Materials Science and Engineering, SUNY at Stony Brook, New York 11794, USA*
[5]*LANSCE, Los Alamos National Laboratory, Los Alamos, New Mexico 87545, USA*

The surface dynamics of supported ultrathin polystyrene films with thickness comparable to the radius of gyration were investigated by surface sensitive x-ray photon correlation spectroscopy. We show for the first time that the conventional model of capillary waves on a viscous liquid has to be modified to include the effects of a shear modulus in order to explain both static and dynamic scattering data from ultrathin molten polymer films.

The dynamical properties of entangled chains in polymer melts have been the subject of much intense study over the past several years [1–4]. Attempting to account for the manner in which the viscosity and the elastic modulus depend on quantities such as the molecular weight, entanglement length, frequency, etc., presents a considerable challenge for theory to explain in detail. The corresponding problem for polymer melts adsorbed on substrates in thin film does not appear to have been addressed. In this Letter, we present the wave vector dependence of the relaxation time for overdamped capillary waves on supported ultrathin molten polystyrene (PS) films [thickness $h \sim R_g - 4R_g$, where $R_g = 6.7(N/6)^{1/2}$ Å is the radius of gyration in θ condition with N being the polymerization index] with different molecular weights by a noninvasive technique: x-ray photon correlation spectroscopy (XPCS). In discussing the dynamics, we also show that our current model explains why earlier measurements of the static scattering function $S(q_\parallel)$ [5] had to be interpreted in terms of brush-like models when the film thickness was comparable to R_g. We have previously demonstrated [6] that the surface dynamics of thin PS ($M_W = 123k$) molten films with thickness $>8R_g$ and wavelengths of order 100 nm or larger could be explained in terms of the normal hydrodynamic theory for capillary wave fluctuations on viscous liquid films. However, our current measurements, which were carried out for a variety of molecular weights of PS, show that when the film thickness h becomes $\sim 2R_g$ the surface fluctuation relaxation times differ significantly from those of a simple viscous liquid. As we will show, this can be attributed to the occurrence of the shear modulus, which presumably arises from the adsorption effect at the substrate. In fact, when $h \sim R_g$ no surface dynamics were seen at all for observable time scales that can be reached in the experiments, i.e., the polymer chains appeared to be immobilized on the substrate.

In order to investigate the effect of viscoelasticity on the surface dynamics of thin liquid polymer films, we calculated the surface dynamic susceptibility by generalizing the linear response theory in Ref. [7] for viscoelastic liquids. In solving the equations of motion, a nonslip boundary condition at the polymer-substrate interface and a solution of monochromatic form $e^{i(kx-\omega t)}$ are assumed. Following Nakanishi and Kubota [8] and Harden *et al.* [9], a constitutive frequency dependent shear modulus $G(\omega) = \mu - i\omega\eta$ is used, where μ is the real and frequency independent shear modulus, and η is the dynamic viscosity. The complete form of a generalized complex dynamic susceptibility $\chi_{zz}(q, \omega)$ is then obtained via the classical fluctuation dissipation theorem. The static fluctuation spectrum was found to be

$$S(q_\parallel) \cong k_B T / [\gamma q_\parallel^2 + 2\mu q_\parallel + 3\mu/(q_\parallel^2 h^3)], \quad (1)$$

where $q_\parallel$ is the in-plane scattering wave vector, γ is the surface tension, and h is the film thickness. Equation (1) is equivalent to the theory by Fredrickson *et al.*, which was obtained by applying equipartition theory to the total free energy of a molten polymer brush film under an arbitrary two-dimensional, low-amplitude distortion [10]. $S(q_\parallel)$ can be directly related to static diffuse scattering [5]. However, we emphasize that the polymer films studied here are not grafted brushes and the shear modulus is expected to be much smaller than that evaluated by Fredrickson *et al.*. In fact, directly applying the results in Ref. [10] to evaluate the shear modulus yields a value several orders of magnitude larger than the measured values for the spun-cast films in our experiments. In the limit that $\gamma \gg \mu h$, Eq. (1) yields a low wave vector cutoff $q_{l,c} = (3\mu/\gamma)^{1/4} h^{-3/4}$ in the transverse diffuse x-ray scattering from thin films [5,11]. Below this cutoff, thermal capillary waves of long wavelength are strongly suppressed. In a similar manner, the van der Waals interactions also introduce a low cutoff

given by $q_{vdW} = (A_{eff}/2\pi\gamma)^{1/2}/h^2$, where A_{eff} is the effective Hamaker constant [12]. In the present case q_{vdW} is much smaller than $q_{l,c}$, so that it can be ignored. In order to obtain the surface tension, static diffuse scattering was measured at very large wave vectors, and capillary wave theory using the distorted wave Born approximation [13,14] was employed. The obtained surface tensions are in agreement with the values given in Refs. [15,16].

In highly viscous polymeric liquids the damping effects are so prominent that all the propagating modes become overdamped. The dynamic spectrum of thermally excited surface waves takes the form of a Lorentzian shape, with the width being the inverse of the characteristic relaxation time,

$$\tau(q_{\parallel}) \cong \frac{\tau_0(q_{\parallel})}{1 + \tau_0(q_{\parallel})(\mu/\eta)}, \qquad (2)$$

where

$$\tau_0(q_{\parallel}) \cong \frac{2\eta[\cosh^2(q_{\parallel}h) + q_{\parallel}^2 h^2]}{\gamma q_{\parallel}[\sinh(q_{\parallel}h)\cosh(q_{\parallel}h) - q_{\parallel}h]}. \qquad (3)$$

There are two asymptotes of the viscoelastic surface dynamic model [Eq. (2)]: $\tau_0(q_{\parallel}) \ll \eta/\mu$ reduces $\tau(q_{\parallel})$ to $\tau_0(q_{\parallel})$, which is the purely viscous model previously used to describe a free liquid surface without elastic effects [6,17]; in the limit that $\tau_0(q_{\parallel}) \gg \eta/\mu$, $\tau(q_{\parallel}) \approx \eta/\mu$, which is a manifestation of viscoelasticity. Such a wave vector independent relaxation was recently observed on PS/PBrS bilayer systems [18,19].

Monodisperse ($M_W/M_N < 1.08$) PS films with various molecular weights [$M_W = (65k, 123k, 400k,$ and $650k)$ g/mol] were spun cast onto 0.5 mm silicon wafers which had been pretreated with piranha etch and dilute HF solution. Film thicknesses were controlled to be R_g, $2R_g$, $4R_g$, and thicker. Samples were then annealed for approximately 24 hours at 170 °C in high vacuum to remove the residual solvent.

Although the elasticity manifests itself in Eq. (2), the limits imposed by the XPCS experimental setup due to weak scattered intensity at high $q_{\parallel}$ and beam line temporal instability prevent a precise determination of the shear modulus directly from the dynamic measurement. Equation (1) points out that the shear modulus can also be determined more accurately from static scattering experiments with a much broader $q_{\parallel}$ window. Transverse diffuse scans were measured at Sector 8-ID-E, Advanced Photon Source (APS), Argonne National Laboratory, on each sample at various temperatures well above the bulk glass transition temperature ($T_g \sim 95$ °C) desired for the XPCS measurement. At a small q_z, the observed intensity with slit widely opened in the direction of out of plane (q_y) is essentially proportional to the convolution of Eq. (1) and the instrumental resolution function [5,14,20]. In Fig. 1, we show the log-log plot of transverse scans for PS (123k) films of thicknesses $2R_g$ and $4R_g$. The fitted low wave-
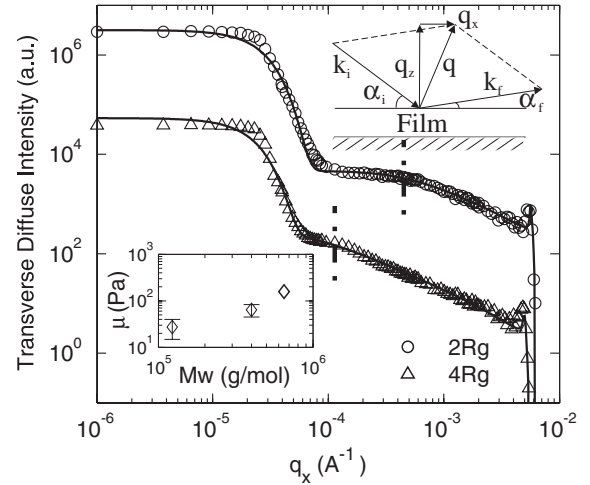
FIG. 1. Transverse diffuse scattering at $q_z = 0.2$ Å^{-1} for PS (123k) films with thickness $2R_g$ and $4R_g$ at 195 °C. Solid lines represent the fits described in the text, and vertical dash-dotted lines indicate the low wave vector cutoffs from the fitting for two films, respectively, $q_{l,c} = 4.51$ and 1.14×10^{-4} Å^{-1}. The upper inset shows the in-plane scattering geometry. The lower inset shows μ versus M_W for $2R_g$ films at 195 °C.

vector cutoff $q_{l,c}$ related to the shear modulus of the film is marked by the vertical dash-dotted lines. In the lower inset, the shear moduli from $2R_g$ films clearly show values at least 3 orders of magnitude smaller than those expected for brushes [10]. The error bars were calculated based on repeated measurements. We found that the cutoff position in the rocking scans shows some variations on repeating the measurements, indicating that the films of $M_W > 123k$ are still in a nonequilibrium state. However, it should not affect the following XPCS dynamic measurements because the process towards the final equilibrium occurs at a very much slower time scale than the capillary wave relaxation.

The XPCS experiments were then performed at Sector 8-ID-I using a partially coherent monochromatic x-ray beam ($E = 7.5$ keV). The scattering geometry has been described elsewhere [6,16]. With the incident angle (0.14°) below the critical angle of total external reflection (0.16°), the electric field intensity decays exponentially (evanescent wave) into the film. Hence, the scattering is basically dominated by the surface contribution. An x-ray CCD camera was mounted 3472 mm downstream to collect the time dependent diffuse scattering. To avoid x-ray radiation damage, samples were translated to a fresh area every 10 min. after exposure. Reflectivity was also performed before and after each measurement in order to check film thickness and radiation damage.

For partially coherent x rays incident at angles less than the critical angle, as shown in Ref. [6], the normalized intensity-intensity autocorrelation function is computed as $g_2(q_{\parallel}, t) = \langle I(q_{\parallel}, t')I(q_{\parallel}, t' + t)\rangle/\langle I(q_{\parallel}, t')\rangle^2$ for each wave vector transfer $q_{\parallel}$, where $I(q_{\parallel}, t')$ is the scattering intensity at $q_{\parallel}$ and at time t', and the angular brackets refer to averages over time t' and t denotes the delay time. g_2

obtained from PS (123k) films with thickness of $4R_g$ and $2R_g$ is shown in Figs. 2(a) and 2(b), respectively, at 195 °C for two different wave vectors 5.4×10^{-4}, 7.7×10^{-4} Å^{-1}. Solid lines are best single-exponential fits, i.e., $g_2 = 1 + \beta \exp(-2t/\tau)$, where β is the speckle contrast and $\tau = \tau(q_\parallel)$ is the relaxation time for equilibrium surface height fluctuations.

In Fig. 3, the relaxation time constant τ deduced from g_2 is plotted as a function of in-plane wave vector $q_\parallel$ for PS films with $2R_g$ thickness and different molecular weights. Both viscoelastic [Eq. (2)] and purely viscous models [Eq. (3)] are used for the fitting. The surface tension is known from the static scattering at very high wave vectors, the film thickness is obtained by fitting the reflectivity, and the shear modulus (or low wave-vector cutoff) is obtained from the transverse diffuse scattering. Hence the viscosity is the only fitting parameter. Obviously the model with the shear modulus provides a better fit. However, when the film thickness is increased to $4R_g$ or greater, the viscous model without the shear modulus describes the surface dynamics sufficiently well [6]. More interestingly, when two films of 65k, $4R_g$ (not plotted) and 400k, $2R_g$ are compared, even though they have similar absolute thickness, their surface dynamics are very different: the latter shows a significant viscoelastic effect, while the former does not. Such an effect was also observed in other $2R_g$ films of different molecular weights, but not in $4R_g$ films. Therefore, it is not the absolute thickness of the film but rather the ratio of the thickness to R_g and the length scale of the surface waves which determine whether the elastic shear modulus needs to be taken into account in calculating the relaxation time of overdamped capillary waves. It is noted that Fig. 3 shows the beginning of a deviation from the surface tension dominated regime at large $q_\parallel$ to the elasticity dominated regime at small $q_\parallel$. However, in order to actually observe a
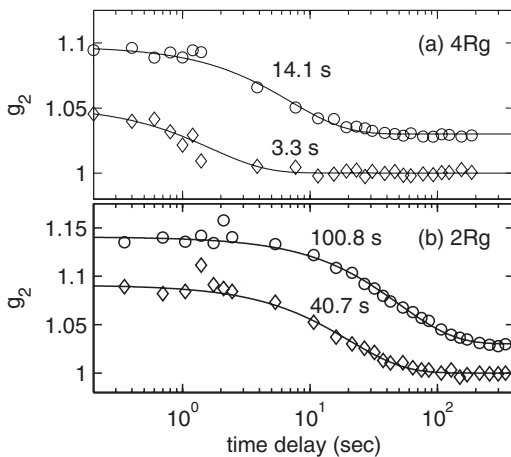
complete crossover regime to where τ reaches the constant limiting value of η/μ, one has to go to very small $q_\parallel$. The shear modulus is weakly dependent on temperature, compared with a larger dependence of viscosity on temperature, which would imply that such a plateau would be temperature dependent. However, this regime is currently inaccessible because the relaxation times become so large that the beam line temporal instability introduces drifts and prevents accurate measurements of time scales beyond ~ 1000 s in a surface reflection geometry. Despite that it is not reachable here and the transition is only partially observed at τ values of hundreds of seconds, the trends in the data (Fig. 3) clearly indicate that the plateau of τ versus $q_\parallel$ curves for lower temperatures occurs at considerably larger τ values.

Although the chains in $2R_g$ films are not purposely grafted, chain segments are confined and still pinned onto the substrate, forming a Guiselin brush [21]. In order to create surface fluctuations and meanwhile maintain a constant density, lateral chain stretching is required. However, due to the large entropic penalty, the long wavelength mode (lateral displacement at a large length scale) would be suppressed [10,22], and the effective elasticity is expected in this regime. This effect does not manifest itself for films with $4R_g$ or larger thickness, partially because for $hq_\parallel \ll 1$, $\tau_0 \sim 1/h^3$, meaning a speed up of a factor of 8 for surface wave relaxation time when thickness increases from $2R_g$ to $4R_g$, so that the second term in the denominator of Eq. (2) may be negligible. Furthermore, in a qualitative way the elasticity due to the adsorption of chain

FIG. 2. g_2 functions obtained from PS (123k) films with thickness (a) $4R_g$, (b) $2R_g$ at 195 °C at wave vector 5.4×10^{-4} Å^{-1} (○), 7.7×10^{-4} Å^{-1} (◇) . Solid lines are best single-exponential fits described in the text, with fitted τ values labeled. For clarity the curves are shifted vertically.
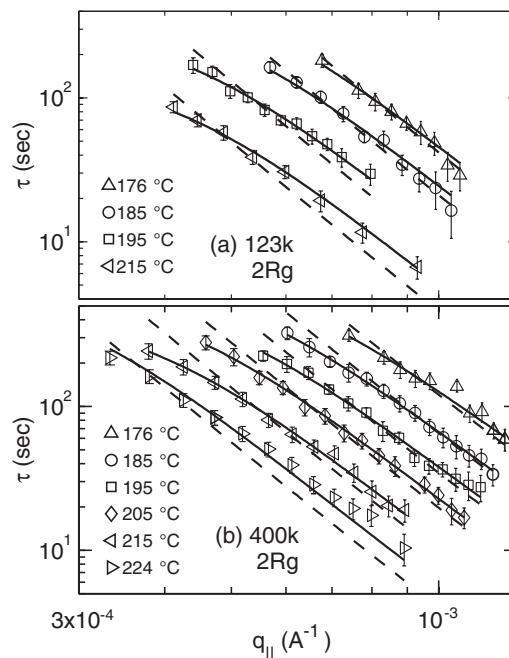
FIG. 3. Measured time constant τ versus in-plane wave vector $q_\parallel$ for $2R_g$ films with molecular weight (a) 123 kg/mol and (b) 400 kg/mol. Solids lines and dashed lines are fits to viscoelastic [Eq. (2)] and viscous [Eq. (3)] models, respectively.
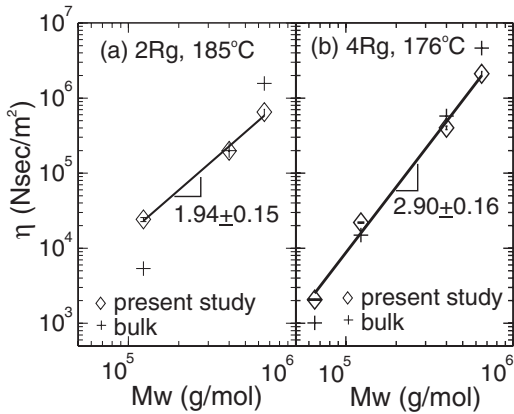
FIG. 4. Viscosity ($\diamond$) as a function of molecular weight for (a) $2R_g$ films at 185 °C and (b) $4R_g$ films at 176 °C. Lines are power-law fits with slopes labeled underneath. Viscosity values for PS bulk (+) are taken from Ref. [25].

segments to the substrate is expected to less effectively modulate the surface dynamics in thicker films. Therefore the capillary wave relaxation becomes less sensitive to the elasticity effect in $4R_g$ within the current experimental time and wave vector windows.

The obtained viscosities from the fits to the viscous model ($4R_g$) and the viscoelastic model ($2R_g$) using the values of μ given by the static $S(q_\parallel)$ are plotted as a function of M_W in Fig. 4. A power-law fitting $\eta \sim M_W^\alpha$ yields $\alpha = 1.94 \pm 0.15$ and 2.90 ± 0.16 for $2R_g$ [Fig. 4(a)] and $4R_g$ [Fig. 4(b)] films, respectively. In strongly confined polymers, the chains are proposed to reduce interpenetration into each other [23], resulting in less entanglement. However, according to Jones et al. [24], this confinement-induced entanglement reduction only occurs when the film thickness is much less than R_g and closer to the segment length. Nevertheless, it is interesting to note that the deviation of the scaling factor α from the prediction of the reptation theory for the bulk 3.0 ~ 3.4 increases as the film thickness becomes smaller relative to R_g.

The surface dynamics of $1R_g$ films were also studied. Inserting the values of the bulk viscosity [25] and surface tension from static scattering measurements into Eq. (3), we obtained a relaxation time for the $1R_g$ film which should have been observable within the experimental time window. However, the observed g_2 of the $1R_g$ film is above unity and shows time independence for all the wave vectors (not plotted here), indicating that the surface fluctuations are very highly temporally correlated, a signature of a static surface or at least a surface with extremely slow dynamics. This might be due to the additional fact that the number of adsorption points per chain should be larger in $1R_g$ films than $2R_g$ films, which means there is highly restricted chain mobilities in $1R_g$ films and the lateral displacement of chains required for surface fluctuations is thermodynamically unfavored.

In summary, we have employed XPCS to measure the surface dynamics of supported polymer films of thicknesses down to close to R_g. In $1R_g$ films, no surface dynamics are observed. Suppressed dynamics are observed for $2R_g$ films, which are analyzed based on viscoelastic calculations. A shear modulus is introduced to account for the effect on the surface dynamics due to the pinning of the polymer chains to the substrate. Surface dynamics from films of thicknesses equal to or thicker than $4R_g$ show a normal viscous behavior within the allowed experimental time window and wave vector range.

[1] P.-G. de Gennes, *Scaling Concepts in Polymer Physics* (Cornell University, Ithaca, NY, 1979).
[2] P.-G. de Gennes and L. Leger, Annu. Rev. Phys. Chem. **33,** 49 (1982).
[3] M. Doi and S. F. Edwards, *The Theory of Polymer Dynamics* (Oxford University, New York, 1986).
[4] S. T. Milner and T. C. B. McLeish, Phys. Rev. Lett. **81,** 725 (1998).
[5] J. Wang et al., Phys. Rev. Lett. **83,** 564 (1999).
[6] H. Kim et al., Phys. Rev. Lett. **90,** 068302 (2003).
[7] J. Jäckle, J. Phys. Condens. Matter **10,** 7121 (1998).
[8] H. Nakanishi and S. Kubota, Phys. Rev. E **58,** 7678 (1998).
[9] J. L. Harden et al., J. Chem. Phys. **94,** 5208 (1991).
[10] G. H. Fredrickson et al., Macromolecules **25,** 2882 (1992).
[11] Y.-S. Seo et al., Phys. Rev. Lett. **94,** 157802 (2005).
[12] J. Israelachvili, *Intermolecular and Surface Forces* (Academic, London, 1992), 2nd ed.
[13] S. K. Sinha et al., Phys. Rev. B **38,** 2297 (1988).
[14] M. K. Sanyal et al., Phys. Rev. Lett. **66,** 628 (1991).
[15] S. Wu, in *Polymer Handbook*, edited by J. Brandrup, E. H. Immergut, and E. A. Grulke (Wiley, New York, 1999), pp. VI–525, 4th ed.
[16] L. B. Lurio et al., Macromolecules **36,** 5704 (2003).
[17] C. Li et al., Macromolecules **38,** 5144 (2005).
[18] X. Hu et al., Phys. Rev. E **74,** 010602 (2006).
[19] Z. Jiang et al., Phys. Rev. E **74,** 011603 (2006).
[20] J. Daillant and A. Gibaud, *X-Ray and Neutron Reflectivity: Principles and Applications* (Springer, New York, 1999).
[21] O. Guiselin, Europhys. Lett. **17,** 225 (1992).
[22] H.-W. Xi and S. T. Milner, Macromolecules **29,** 4722 (1996).
[23] K. Binder, Physica (Amsterdam) **200A,** 722 (1993).
[24] R. L. Jones et al., Nature (London) **400,** 146 (1999).
[25] D. J. Plazek and V. M. O'Rourke, J. Polym. Sci., A-2 **9,** 209 (1971).